Available online at www.sciencedirect.com
SCIENCE DIRECT®
Journal of Sound and Vibration 276 (2004) 157–179
JOURNAL OF SOUND AND VIBRATION
www.elsevier.com/locate/jsvi

Active vibration isolation using an inertial actuator with local force feedback control

L. Benassi*, S.J. Elliott, P. Gardonio

Institute of Sound and Vibration Research, University of Southampton, Southampton SO17 1BJ, UK

Received 23 May 2003; accepted 24 July 2003

Abstract

The design of inertial actuators with local force feedback control and their use in active vibration isolation systems is considered. Unlike reactive actuators, inertial actuators do not need to react off a base structure and can therefore be directly installed on a vibrating structure. In order to guarantee good stability margins in the active isolation controller, however, the actuator resonance must have a low natural frequency and it must be well damped.

The behaviour of an inertial actuator with different local force feedback control schemes is first analysed, and it is shown that a phase-lag controller has a good stability margin and can effectively damp the actuator resonance using relatively low gains, compared with a direct force feedback or integrated force feedback controller.

A frequency-domain formulation is then used to analyse the stability and performance of an active isolation system using an inertial actuator with local force feedback control and an outer velocity feedback control loop. The plant response, from force actuator input to sensor output, is derived in terms of the mechanical mobilities of the equipment structure being isolated and the vibrating base structure, and the mechanical impedance of the intervening mount.

An experimental study of active vibration isolation using an inertial actuator with local feedback control was then carried out. Theory and experiments agree well, demonstrating the effectiveness of the phase-lag controller. However, the need to have an inertial actuator with a low resonance frequency leads to problems with static deflections.

1. Introduction

A problem that arises in several application areas is the isolation of sensitive equipment from vibration of the base structure to which it is attached. The isolation of any vibration-sensitive

*Corresponding author. Tel.: +44-23-8059-2689; fax: +44-23-8059-3190.
E-mail address: lb@isvr.soton.ac.uk (L. Benassi).

0022-460X/$ - see front matter
doi:10.1016/j.jsv.2003.07.019

equipment from base vibration is usually achieved using resilient mounts. However, with such passive mounts there is a trade-off between low- and high-frequency isolation performances depending on the damping of the mount. A major challenge is to make the mount as stiff as possible, statically, to better support the equipment, and dynamically as soft as possible, to better isolate the equipment. This is difficult to accomplish with passive elastometric mounts, as described by Crede [1] and Ungar [2].

To provide a more favourable static and dynamic stiffness compromise, active isolation solutions such as skyhook damping [3] must be used, which are usually based on mounts and actuators. This paper is specifically concerned with the use of inertial actuators in active vibration isolation systems. Inertial actuators do not need to react off a base structure, so they can be used as modules that can be directly installed on a vibrating structure. It has previously been shown, however, that in order to implement stable skyhook damping with an inertial actuator, the natural frequency of the actuator must be below the first resonance frequency of the structure under control and the actuator resonance should be well damped [4].

In Section 2 the dynamic model of a typical inertial actuator is described and its blocked response and mechanical impedance are derived.

In Section 3 a theoretical analysis of an inertial actuator with local force feedback control is presented. In particular, direct force feedback control, integrated force feedback control and an intermediate solution based on a phase-lag compensator are discussed. It is found that this latter solution gives the closed-loop system a good stability margin and good performance.

In Section 4 the active vibration isolation problem is investigated using the locally controlled inertial actuator. The Nyquist plot and frequency response are discussed for a particular case in which a rigid equipment structure is resiliently mounted on a vibrating flexible base.

In Section 5 experiments are described that support the theoretical findings and finally in Section 6 some overall conclusions are drawn.

2. Inertial actuator response

An inertial actuator is a mass supported on a spring and driven by an external force. The force in small actuators is normally generated electromagnetically. The suspended mass can either be the magnets with a supporting structure or in some cases the coil itself. The transduction mechanism which would supply the force to the system is not modelled in detail because its internal dynamics are typically well beyond the bandwidth of the structural response. Unlike reactive actuators, inertial actuators do not need to react off the base structure, so they can be used as modules that can be directly installed on a vibrating structure. This feature makes them very useful.

A mechanical model of an inertial actuator is shown in Fig. 1. A mass is suspended on a spring and a damper, and in parallel with them, an actuator force f_a drives the mass. v_a and v_e are, respectively, the moving mass velocity and the base velocity. The equation describing the dynamics of the system in Fig. 1 is given by

$$j\omega m_a v_a + c_a(v_a - v_e) + k_a(v_a - v_e)/j\omega = -f_a, \tag{1}$$

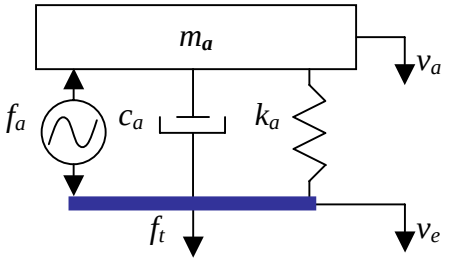

Fig. 1. Mechanical model and sign convention of an inertial actuator.

where v_a and v_e are complex velocities. Important parameters in characterizing the behaviour of an inertial actuator are its resonance frequency, which is given by

$$\omega_a = \sqrt{\frac{k_a}{m_a}} \tag{2}$$

and the actuator damping ratio, defined as

$$\zeta_a = \frac{1}{2}\frac{c_a}{\sqrt{k_a m_a}}. \tag{3}$$

The transmitted force f_t is a linear function of the actuator force f_a and the equipment velocity v_e, and may be written as

$$f_t = T_a f_a - Z_a v_e, \tag{4}$$

where

$$T_a = \frac{-\omega^2 m_a}{k_a - \omega^2 m_a + \mathrm{j}\omega c_a} \tag{5}$$

is the blocked response of the actuator and

$$Z_a = \frac{\mathrm{j}\omega m_a k_a - \omega^2 m_a c_a}{k_a - \omega^2 m_a + \mathrm{j}\omega c_a} \tag{6}$$

is its mechanical impedance. The blocked response of a typical actuator with $\zeta_a = 4.7\%$ is illustrated in Fig. 2, showing the resonance at its natural frequency. At high frequency this response tends to unity, with no phase shift, indicating that the transmitted force f_t follows the actuator force f_a since the mass provides a stable inertial platform to react the force. The mechanical input impedance of the actuator, as plotted in Fig. 3, is mass-controlled at low frequency, stiffness controlled at higher frequency and at the resonance frequency is dominated by the actuator's damping.

Depending on the actuation orientation with respect to gravity, or other static accelerations, the effective stroke of the actuator can be reduced as the suspended mass is forced closer to one end stop. The worst case is when the actuator output axis is aligned with the local static acceleration field, which is the case for the problem analysed in this work. The magnitude of the gravity-induced sag is proportional to the inverse of the square of the actuator's resonance frequency [2]. Consequently the lower the resonance frequency, the greater the sag.

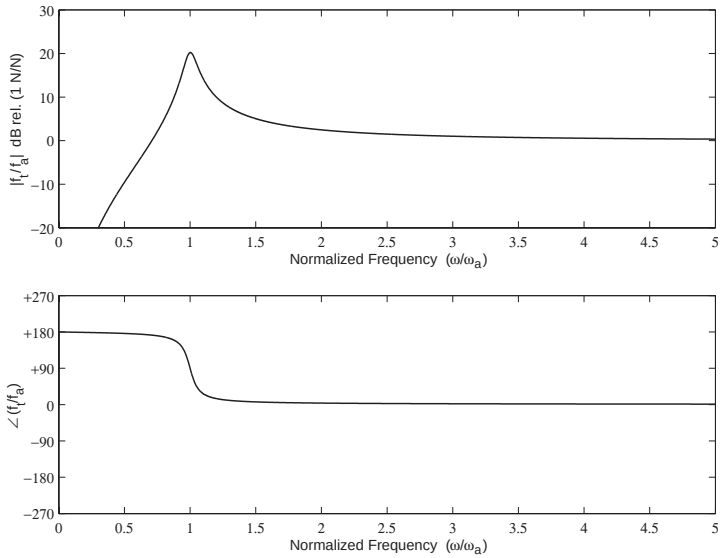

Fig. 2. Blocked response, transmitted force per unit actuator force, of the inertial actuator as a function of normalized frequency.

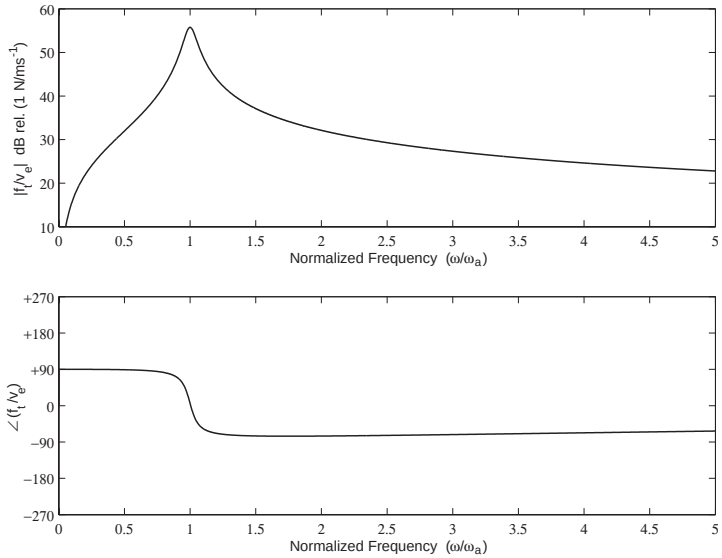

Fig. 3. Mechanical input impedance, reaction force per unit imposed velocity, of the inertial actuator as a function of normalized frequency.

3. Inertial actuator with local force feedback

The inertial actuator with local force feedback control is shown schematically in Fig. 4. The transmitted force f_t is measured and fed back to the inertial actuator through a feedback controller with frequency response $H(\mathrm{j}\omega)$. The command signal f_c can be considered, in control

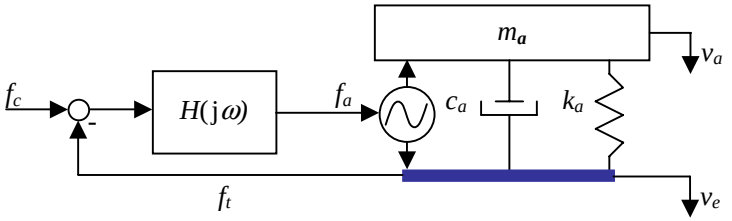

Fig. 4. Schematic of an inertial actuator with local force feedback control.

terms, as the reference point [5]. In this section the stability and performance of the actuator with various types of local force feedback will be discussed.

3.1. Direct force feedback control

If $H(j\omega) = h_f$, where h_f is a positive constant, direct force feedback is implemented. The Nyquist plot of the open-loop response of the blocked actuator is shown in Fig. 5, which allows the relative stability of the system to be assessed [5]. Direct force feedback control is seen to be unconditionally stable in this ideal case since for no feedback gain would the Nyquist plot enclose the $(-1, 0)$ point. At low frequency, the Nyquist plot does lie very close to the real axis, however, and therefore instability is likely to occur at high gains in real systems where an additional low-frequency phase shift may be present due to the electronic components [6,7]. It can also be noted that at high frequency the Nyquist plot does not go to the origin and this is due to the fact that the magnitude in the corresponding Bode plot (Fig. 2) tends to a constant.

An important assumption that underlies the result shown in Fig. 5 is that the supporting structure which the inertial actuator is attached to is assumed to be perfectly rigid. For a more general analysis equation (4) can be expanded with the base velocity v_e written in terms of the input mobility of the structure Y_e as

$$v_e = Y_e f_t. \tag{7}$$

Substituting Eq. (7) into Eq. (4) the plant transfer function in this case, between actuator force f_a and transmitted force f_t, is given by

$$G_f = \frac{f_t}{f_a} = \frac{T_a}{1 + Z_a Y_e}. \tag{8}$$

The difference between the blocked plant response, T_a, and that when it is loaded by the structure, is the factor $(1 + Z_a Y_e)^{-1}$. If the structure is vibrating with velocity v_{ep} before the actuator is attached, its velocity after the actuator has been attached is given by

$$v_e = v_{ep} + Y_e f_t. \tag{9}$$

Assuming that the actuator is undriven, $f_a = 0$, then f_t from Eq. (4) will be equal to $-Z_a v_e$. Substituting this into Eq. (9), the fractional change in the structure's velocity due to the attachment of the undriven actuator (i.e., its passive effect on the structure's vibration) is given by

$$\frac{v_e}{v_{ep}} = \frac{1}{1 - Y_e Z_a}, \tag{10}$$

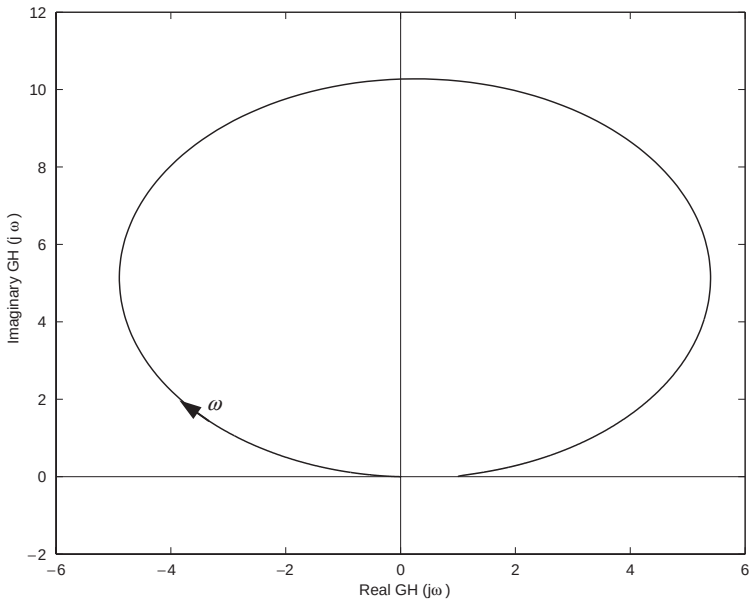

Fig. 5. Nyquist plot of the open-loop response for the inertial actuator with direct force feedback ($h_f = 1$), attached to a rigid structure.

which provides some physical interpretation of the effect of the mobility of the structure on the inertial actuator's plant response with local force feedback. The reciprocal frequency response of the plant in the case of direct force feedback control, from Eq. (8), can be written as

$$G_f^{-1} = T_a^{-1}[1 + Z_a Y_e]. \tag{11}$$

The reciprocal of the blocked actuator response T_a (Fig. 2) has a phase shift between 0° and $+180^\circ$. Both Z_a and Y_e are passive terms and thus their individual phase shift is between $\pm 90^\circ$. Consequently, $Z_a Y_e$ and thus $[1 + Z_a Y_e]$ could vary between $\pm 180^\circ$. The overall phase shift of Eq. (8) can therefore, in general, range between -180° and $+360^\circ$; and so in the most general case a constant gain feedback loop is only conditionally stable. In the case of the ideal inertial actuator, however, the phase of Z_a is restricted to being between 0° and $+90^\circ$ below its natural frequency and between -90° and 0° above its natural frequency. One of the applications of the device described in this section, as will be discussed in Section 4, is the vibration isolation of a sensitive piece of equipment using an outer velocity feedback loop to provide skyhook damping. In order to implement a stable outer closed-loop system with an inertial actuator, the actuator resonance must be below the first resonance frequency of the structure under control [4]. The modification of the plant response due to loading by the structure is not as severe in this case as in the most general case described above. For example the Nyquist plot of a system composed of an inertial actuator with direct force feedback control mounted on a rigid piece of equipment, which is connected to a vibrating base through a resilient mount, is shown in Fig. 6, in which the natural frequency of the equipment on its resilient mount is about twice the actuator's natural frequency and the specific values of the parameters used in the simulations have been taken from Table 1. The phase shift of the plant is again restricted to between 0° and $+180^\circ$, with the first loop, at low

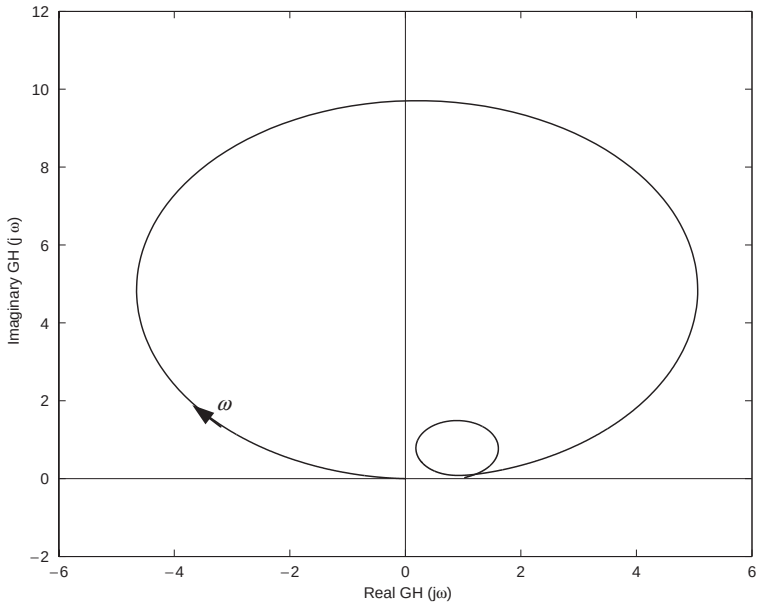

Fig. 6. Nyquist plot of the open-loop response for the inertial actuator with direct force feedback ($h_f = 1$), attached to a flexible structure.

frequency, determined by the behaviour of the inertial actuator, while the smaller loop, at higher frequency, describes the dynamic loading effect of the equipment on its resilient mount on the actuator.

The secondary force f_a for the direct force feedback system shown in Fig. 4 is given by

$$f_a = h_f(f_c - f_t), \tag{12}$$

which when substituted into Eq. (4) and expanded, provides the closed-loop transmitted force as a function of the control command, f_c, and the equipment velocity, v_e. This is given by

$$f_t = \frac{-\omega^2 m_a h_f}{k_a + \mathrm{j}\omega c_a - \omega^2 m_a(1+h_f)} f_c - \frac{\mathrm{j}\omega m_a k_a - \omega^2 m_a c_a}{k_a + \mathrm{j}\omega c_a - \omega^2 m_a(1+h_f)} v_e. \tag{13}$$

The closed-loop response of the actuator with direct force feedback is given by the transmitted force f_t per unit control command f_c, as plotted in Fig. 7. The assumed parameters of the system are given in Table 1. When the local feedback gain h_f increases, the transmitted force tends to the control command f_c. This means that the transmitted force can be regulated using the command signal f_c. A second important aspect is that when the feedback gain h_f increases, the actuator resonance is shifted to lower frequencies, while its magnitude increases. The transmitted force f_t is proportional to the acceleration of the moving mass m_a and consequently direct force feedback is equivalent to feeding back the acceleration of the moving mass. Direct force feedback control can thus be interpreted physically as adding an ''apparent'' mass to the inertial actuator moving mass [8]. Although this lowering of the actuator's natural frequency is desirable when used for active

Table 1
Values used in the simulations

Inertial actuator moving mass	$m_a = 0.91$ kg
Inertial actuator damping factor	$c_a = 5.8$ N/m s^{-1}
Inertial actuator spring stiffness	$k_a = 3900$ N/m
Equipment mass	$m_e = 1.08$ kg
Passive mount damping factor	$c_m = 18$ N/m s^{-1}
Passive mount spring stiffness	$k_m = 20{,}000$ N/m
Vibrating plate	See Ref. [8]

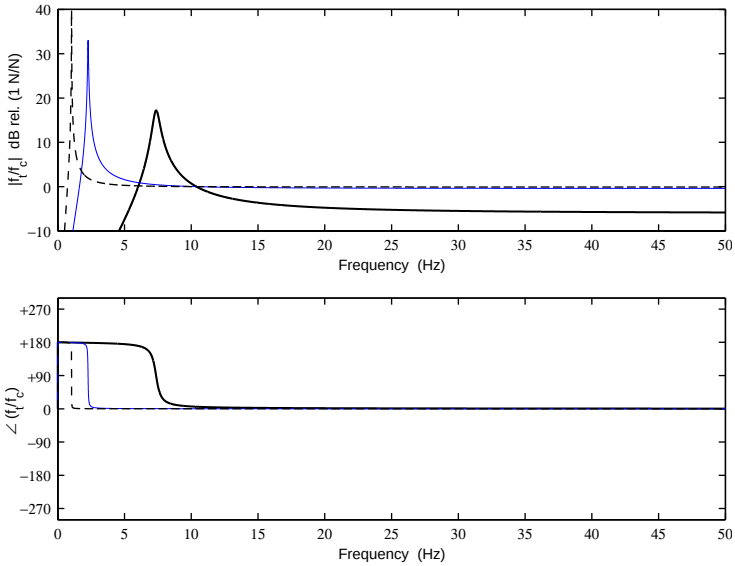

Fig. 7. Transmitted force per unit control command for the inertial actuator with local force feedback when different feedback gains h_f are used: $h_f = 1$ (solid), $h_f = 20$ (faint), and $h_f = 100$ (dashed).

isolation, it makes the stability of the inner feedback loop even more sensitive to low-frequency phase shifts.

Fig. 8 shows the transmitted force f_t per unit equipment velocity, v_e, which is equal to the impedance of the actuator with direct force feedback. The lowering of the resonance frequency can again be observed. It can also be seen that as the feedback gain h_f is increased, the actuator's impedance becomes smaller, particularly at high frequencies, as predicted by Eq. (13).

3.2. Integrated force feedback control

If the local feedback controller in Fig. 4 is given by $H(j\omega) = h_{if}/j\omega$, then integrated force feedback control is implemented. The effect of an integrator in the feedback loop is to rotate the Nyquist plot of the plant response by 90° clockwise. The Nyquist plot of the open-loop response for the actuator with integral force feedback on a rigid base, for example, is shown in Fig. 9, which

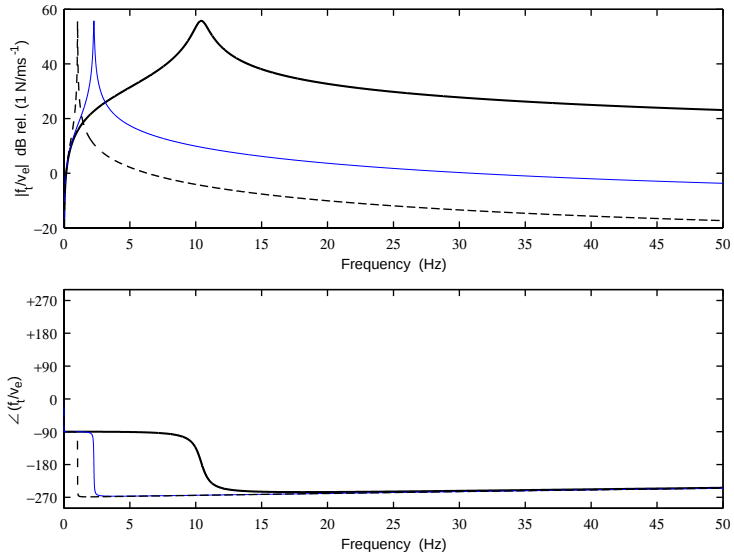

Fig. 8. Frequency response of the actuator's mechanical impedance when $h_f = 0$ (solid), $h_f = 20$ (faint), and $h_f = 100$ (dashed).

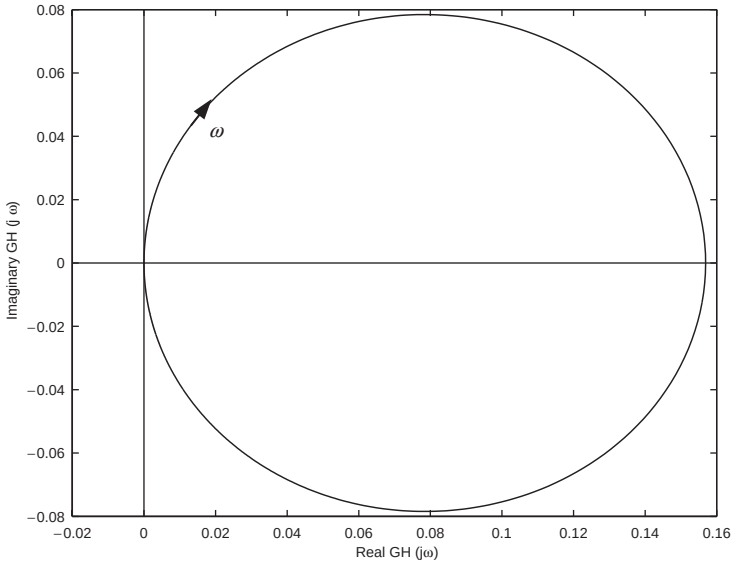

Fig. 9. Nyquist plot of the open-loop response of the inertial actuator with local integral force feedback $H(\mathrm{j}\omega) = h_{if}/\mathrm{j}\omega$, with $h_{if} = 1$, on a rigid structure.

is a rotated version of Fig. 5. The Nyquist plot now lies entirely on the right-hand side of the complex plane, so that this control system is inherently more robust than direct force feedback. In particular low-frequency phase shifts, due to conditioning electronics, of up to $+90^\circ$ will not destabilize the system. Also high-frequency perturbations of the plant response due to the finite

mobility of the structure under control, as discussed above, will not destabilize the system since for the isolation example, whose effect on force feedback was shown in Fig. 6, the Nyquist plot will still be on the right-hand side of the complex plane with integral force feedback. The actuator force in this case is given by

$$f_a = \frac{h_{if}}{\mathrm{j}\omega}\,\omega_1(f_c - f_t), \tag{14}$$

where ω_1 is introduced to ensure that h_{if} is dimensionless, and is assumed to have the value 138.2 rad/s for reasons that will be evident below. When Eq. (14) is substituted into Eq. (4), the transmitted force becomes

$$f_t = \frac{\mathrm{j}\omega m_a h_{if}}{k_a + \mathrm{j}\omega c_a - \omega^2 m_a + \mathrm{j}\omega m_a h_{if}} f_c - \frac{\mathrm{j}\omega m_a k_a - \omega^2 m_a c_a}{k_a + \mathrm{j}\omega c_a - \omega^2 m_a + \mathrm{j}\omega m_a h_{if}}\, v_e. \tag{15}$$

The blocked response of the actuator, the transmitted force f_t per unit control command f_c, with integral force feedback is plotted in Fig. 10. Unlike the previous case, the resonance frequency does not change significantly when the feedback gain increases, although f_t does tend to f_c when very high gains are implemented. For relatively low values of the feedback gain, however, the magnitude falls off above the resonance frequency and a phase shift occurs. Compared to the force feedback control, as shown in Fig. 7, in which the closed-loop response tends to unity with no phase shift at higher frequencies even for moderate feedback gains, higher integral feedback gains are needed with this control strategy in order to obtain the same levels of transmitted force.

Fig. 11 shows the frequency response of the actuator's mechanical impedance, f_t/v_e, for different feedback gains h_{if}. When the feedback gain h_{if} is increased, the impedance is reduced at the resonance frequency and for very high values of feedback gain the magnitude is reduced over

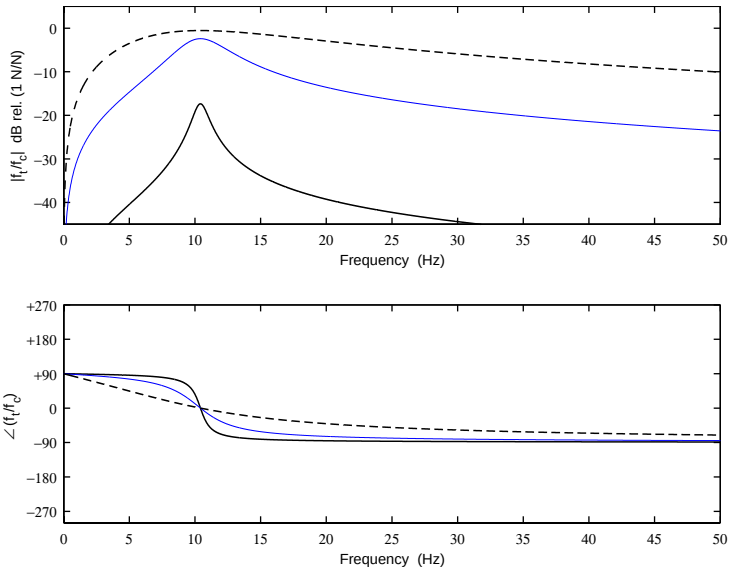

Fig. 10. Transmitted force per unit control command for the inertial actuator with local integral force feedback when different feedback gains h_{if} in $H(\mathrm{j}\omega) = h_{if}\omega_1/\mathrm{j}\omega$ are used: $h_{if} = 1$ (solid), $h_{if} = 20$ (faint), and $h_{if} = 100$ (dashed).

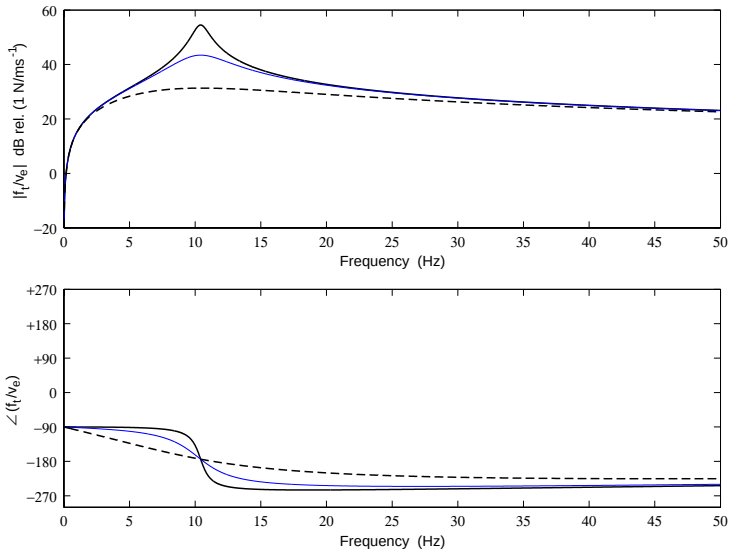

Fig. 11. Frequency response of the actuator's mechanical impedance when $h_{if} = 0$ (solid), $h_{if} = 20$ (faint), and $h_{if} = 100$ (dashed).

the whole frequency range shown in Fig. 11. The physical interpretation of this behaviour is that the integral of the transmitted force is proportional to the velocity of the actuator's mass, and integral force feedback thus adds damping to the system.

The direct force feedback control of the actuator thus does not guarantee a good stability margin at low frequency whereas with integral force feedback large feedback gains are required for good performance at high frequencies. It would therefore be a good idea to alter the local feedback loop in such a way that it behaves like a force feedback controller at frequencies higher than a certain appropriate value and it behaves like an integrated force feedback controller at low frequencies, as will be discussed in the next section.

3.3. Phase-lag compensator

The frequency response of a phase-lag compensator, $H(j\omega) = h_{pl}((j\omega + \omega_1)/j\omega)$, is plotted in Fig. 12 for the case where $\omega_1 = 138.2$ rad/s. If this is used as the local controller in Fig. 4, the Nyquist plot of the open-loop system is shown in Fig. 13. The stability of the closed-loop system is between the behaviour of the previous two cases. In particular, at low frequency the stability margin of the closed-loop system is almost as good as the integrated force feedback case and this is due to the -90° phase shift that the phase-lag controller adds to the plant response at low frequency. At higher frequencies the controller does not add any additional phase shifts and the behaviour of the plant is preserved. The stability of the control system also preserves its robustness when the controller is attached to a flexible structure, since it will affect the Nyquist plot in a similar way to that shown in Fig. 6.

The value of ω_1 is chosen in order to provide a reasonable trade-off between stability of the overall system (especially at low frequency) and its performance. Since the inertial actuator resonance frequency is responsible for the conditional stability of the system, by adding an

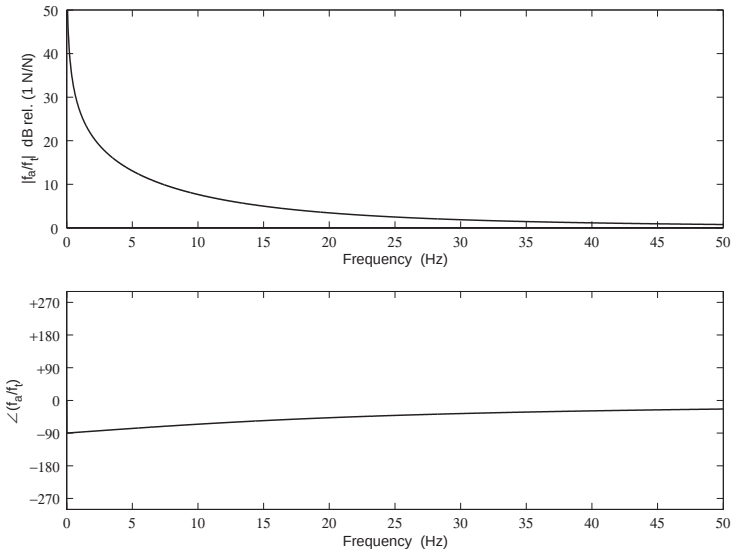

Fig. 12. Frequency response of the phase-lag compensator $H(j\omega) = h_{pl}(j\omega + \omega_1)/j\omega$, with $h_{pl} = 1$ and $\omega_1 = 138.2$ rad/s.

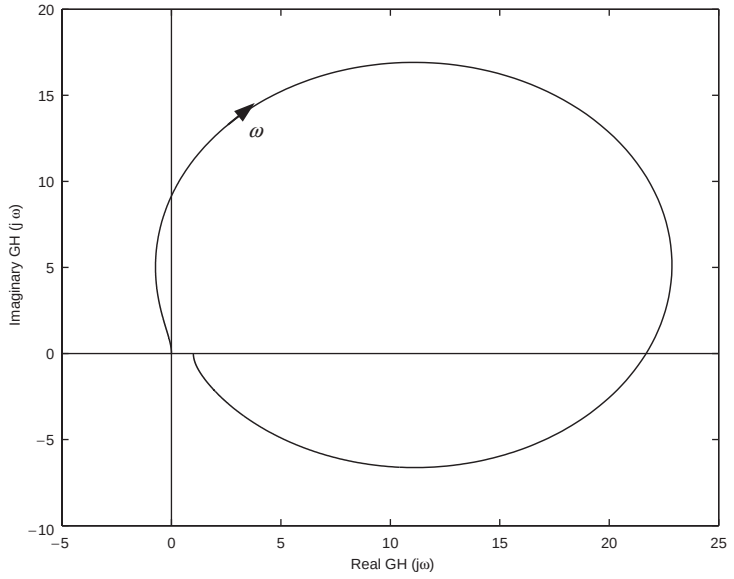

Fig. 13. Nyquist plot of the blocked actuator response when the phase-lag compensator $H(j\omega) = h_{pl}(j\omega + \omega_1)/j\omega$ is implemented, with $h_{pl} = 1$ and $\omega_1 = 138.2$ Hz.

integrator to the feedback loop, the corresponding portion in the Nyquist plot is rotated by 90° clockwise, leading the closed-loop system away from a potential instability. In order to guarantee this feature, ω_1 must be greater than the inertial actuator resonance frequency. On the other hand, in order to guarantee good performance, ω_1 should be small, such that the closed loop system can

benefit from the local force feedback controller. In this study, ω_1 was chosen to be $2\pi \cdot 22 = 138.16$ rad/s, where 22 Hz corresponds to the equipment-dominated resonance frequency of the vibration isolation problem discussed in Section 4. A detailed discussion on the appropriate choice of ω_1 is given in Ref. [8].

The actuator force in this case is given by

$$f_a = h_{pl}\frac{j\omega + \omega_1}{j\omega}(f_c - f_t). \tag{16}$$

Substituting this into Eq. (4), the transmitted force becomes

$$f_t = \frac{-\omega^2 m_a h_{pl} + j\omega m_a h_{pl}\omega_1}{k_a + j\omega c_a - \omega^2 m_a(1 + h_{pl}) + j\omega m_a h_{pl}\omega_1} f_c - \frac{j\omega m_a k_a - \omega^2 m_a c_a}{k_a + j\omega c_a - \omega^2 m_a(1 + h_{pl}) + j\omega m_a h_{pl}\omega_1} v_e, \tag{17}$$

which can be written in the compact form

$$f_t = T'_a f_c - Z'_a v_e \tag{18}$$

where T'_a and Z'_a are the blocked response and mechanical impedance of the actuator, as modified by the local force feedback. Fig. 14 shows the transmitted force per unit control command. As the feedback gain h_{pl} increases, f_t tends to f_c at all frequencies. Compared to the previous control scheme (Fig. 10), at frequencies higher than the resonance frequency, the magnitude is more level, indicating a better performance at high frequency since f_t is closer to f_c than in the previous case. Also, unlike the previous case, there is a smaller phase-lag at frequencies higher than the resonance frequency.

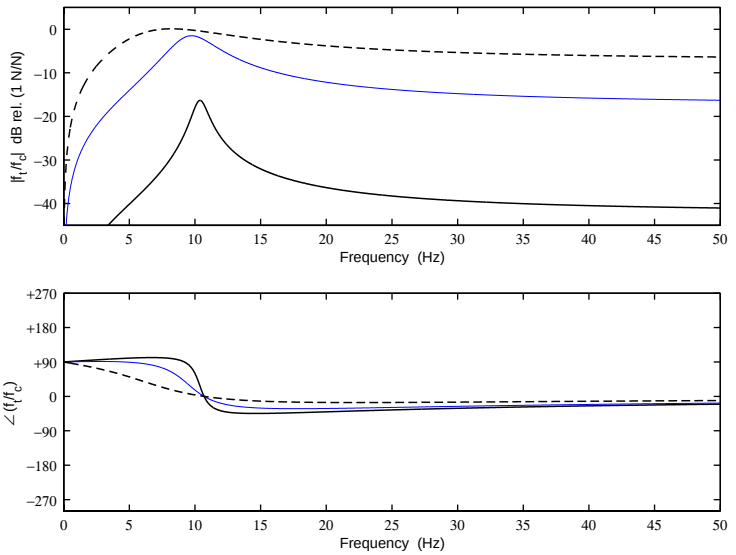

Fig. 14. Transmitted force per unit control command when different feedback gains h_{pl} in the phase-lag compensator are used: $h_{pl} = 1$ (solid), $h_{pl} = 20$ (faint), and $h_{pl} = 100$ (dashed).

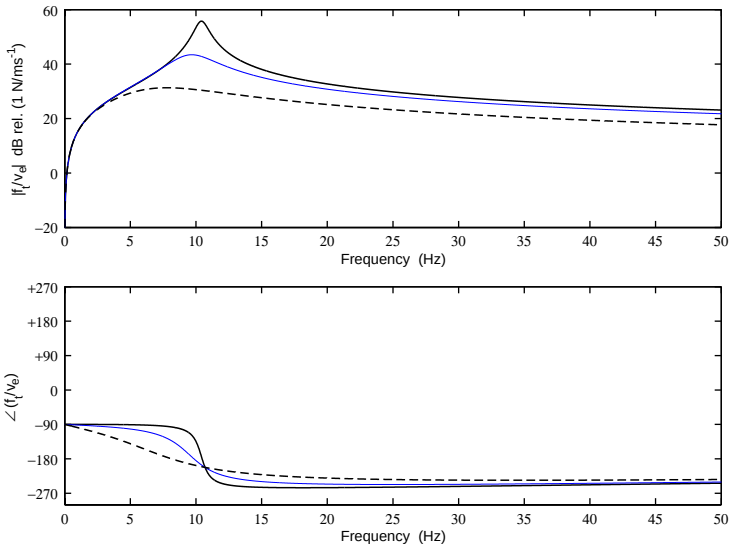

Fig. 15. Frequency response of the impedance when $h_{pl} = 0$ (solid), $h_{pl} = 20$ (faint), and $h_{pl} = 100$ (dashed).

Fig. 15 shows the frequency response of the actuator's mechanical impedance for different feedback control gains h_{pl}. When the feedback gain h_{pl} increases, the impedance f_t/v_e tends to zero, but this is only achieved for large values of the gain. Otherwise, the behaviour is similar to the previous case. Compared to the uncontrolled case (solid line), when the controller is activated the first resonance is no longer present in the impedance equation. This can be physically explained considering the fact that when the feedback gain h_{pl} in the phase-lag compensator increases, the closed-loop system tends to an equivalent system in which the inertial actuator has been removed.

4. Active isolation with the modified inertial actuator

In this section the use of an inertial actuator with local feedback for the active isolation of a rigid equipment structure supported on a flexible base by a resilient mount is considered. The arrangement is illustrated in Fig. 16, and is described fully by Benassi et al. [8]. It consists of a flexible steel base plate 700 mm × 500 mm × 2 mm thick, clamped on the two longer sides, which supports a rigid equipment structure modelled as a point mass on which is mounted an inertial actuator. The equipment structure is supported by a mount, which has a stiffness, k_m, and damping, c_m. The values of the parameters used in the simulations have been taken from Table 1. The model assumes that the system is divided into four elements: a vibrating plate acting as the base structure, a passive mount, the equipment, and the inertial actuator. The actuator has a resonance frequency of about 10 Hz and has a damping ratio of about $\zeta = 4.5\%$, the mounted equipment has a resonance frequency of about 21.5 Hz and a damping ratio of about $\zeta = 5.2\%$, and the vibrating base has a first resonance frequency of about 44.8 Hz and a damping ratio of about $\zeta = 4.8\%$. An inner force feedback loop is used to modify the response of the inertial actuator and an outer velocity feedback system is used to provide active skyhook damping for the

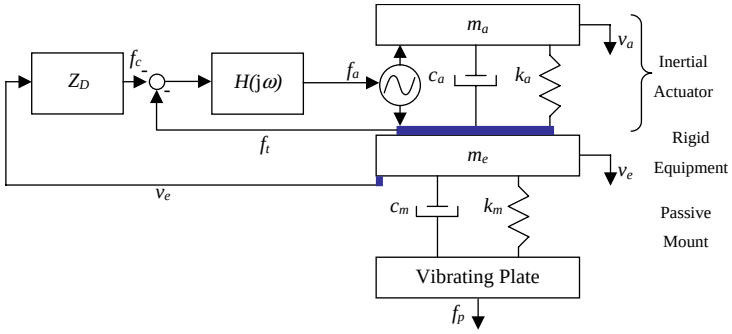

Fig. 16. Schematic of a vibration isolation system with an inertial actuator with inner transmitted force feedback control, and an outer velocity feedback control system.

equipment, also illustrated in Fig. 16. In this study it has been assumed that the actuator resonance frequency is smaller than the equipment natural frequency. When the inertial actuator resonance frequency is greater than the equipment natural frequency, the overall system is more difficult to control and the control strategies presented here do not give good results [8,9].

The expression for the equipment velocity as a function of the primary force f_p and the transmitted force f_t, when a local force feedback control and an outer velocity feedback loop is implemented, is given by

$$v_e = \frac{Y_e Z_m Y_b}{1 + Z_m(Y_e + Y_b)} f_p + \frac{Y_e(1 + Y_b Z_m)}{1 + Z_m(Y_e + Y_b)} f_t, \tag{19}$$

where Y_e is the mobility of the equipment structure, Y_b is the mobility of the base structure and Z_m is the mechanical impedance of the mount. Since the equipment structure is assumed to behave entirely like a rigid body of mass, m_e, its input mobility is equal to $Y_e = 1/(\mathrm{j}\omega m_e)$. The mount is assumed to have a negligible mass, and so without loss of generality its impedance can be written as

$$Z_m = \frac{k_m}{\mathrm{j}\omega} + c_m, \tag{20}$$

where k_m is the mount's stiffness and c_m its damping factor, both of which may be frequency dependent. It can be shown [8] that inner force and outer velocity feedback control does not guarantee a good stability margin, but it performs very well. On the other hand, integrated inner force and outer velocity control is more stable, but it requires higher gains in order to achieve comparable performance. The implementation of a phase-lag controller within the local feedback loop and an outer velocity feedback control loop seems to be an effective compromise between these two approaches. Substituting Eq. (18) into Eq. (19), the expression for the equipment velocity is given by

$$v_e = \frac{Y_e Z_m Y_b}{1 + Z_m(Y_e + Y_b + Y_e Z'_a Y_b) + Y_e Z'_a} f_p + \frac{Y_e T'_a(1 + Y_b Z_m)}{1 + Z_m(Y_e + Y_b + Y_e Z'_a Y_b) + Y_e Z'_a} f_c. \tag{21}$$

If the control law of the outer feedback loop is assumed to take the form $f_c = -Z_D v_e$, where Z_D can be interpreted as the desired impedance of the outer feedback system, then Eq. (21) can be

used to derive the equipment velocity per primary force with both feedback loops as given by

$$v_e = \frac{Y_e Z_m Y_b}{1 + Z_m(Y_e + Y_b + Y_e Z'_a Y_b) + Y_e Z'_a + Y_e T'_a(1 + Y_b Z_m) Z_D} f_p. \tag{22}$$

The stability of the outer loop can be assessed from Fig. 17, which shows the Nyquist plot of the open-loop response of the outer feedback loop, for an inner feedback gain of $h_{pl} = 100$, with the phase-lag controller and an outer feedback gain of $Z_D = 1$. Fig. 18 shows the equipment velocity per unit primary excitation for different gains in the outer feedback loop. The "passive" effect of the inertial actuator with local feedback on the equipment dynamics can be seen from the response with $Z_D = 0$, which shows almost no resonance near the actuator's natural frequency. Good vibration isolation conditions can be achieved at the mounted natural frequency of the equipment. This is due to the fact that at higher frequencies the inertial actuator behaves as an almost perfect force source. The system with both inner and outer feedback loops thus has a good stability margin and it performs well. The mechanical impedance of the actuator when both inner force and outer velocity feedback loops are implemented is given by

$$Z = \frac{\mathrm{j}\omega m_a(k_a + h_{pl}\omega_1 Z_D) - \omega^2 m_a(c_a + h_{pl} Z_D)}{k_a + \mathrm{j}\omega c_a - \omega^2 m_a(1 + h_{pl}) + \mathrm{j}\omega m_a h_{pl}\omega_1}, \tag{23}$$

which is plotted in Fig. 19 for an inner phase-lag controller gain of $h_{pl} = 100$ and an outer velocity gain of $Z_D = 100$. It can be noted that the actuator impedance $Z = f_t/v_e$ tends to the desired impedance, Z_D, past the first resonance frequency, which indicates that the overall system of the inertial actuator with both feedback loops tends to a skyhook damper, as required.

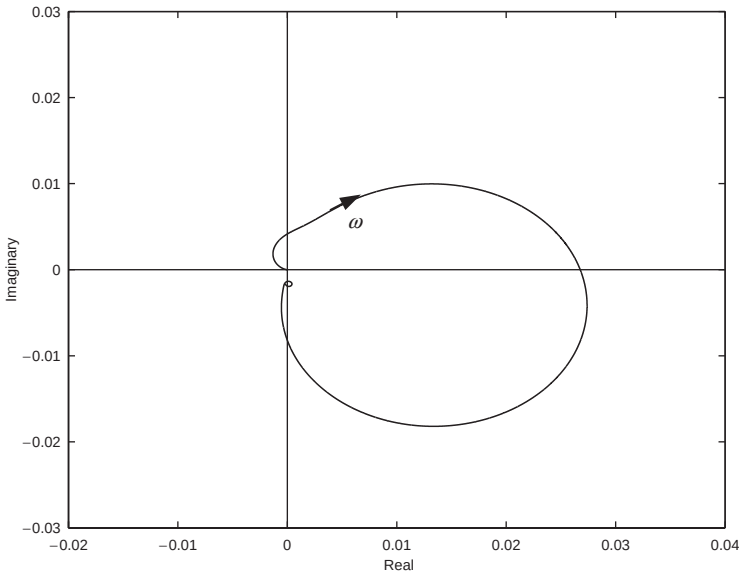

Fig. 17. Nyquist plot of the open-loop response of the outer feedback loop with the phase-lag compensator having a gain $h_{pl} = 100$, implemented as the inner feedback loop, and the outer feedback loop gain of $Z_D = 1$.

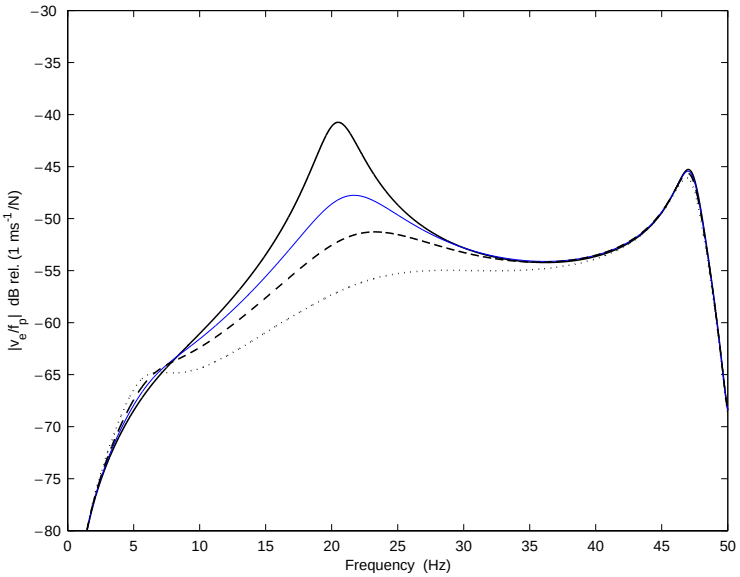

Fig. 18. Equipment velocity per primary excitation when the local feedback loop gains $h_{pl} = 100$ and different outer velocity feedback control gains are used: $Z_D = 0$ (solid), $Z_D = 50$ (faint), $Z_D = 100$ (dashed), and $Z_D = 200$ (dotted).

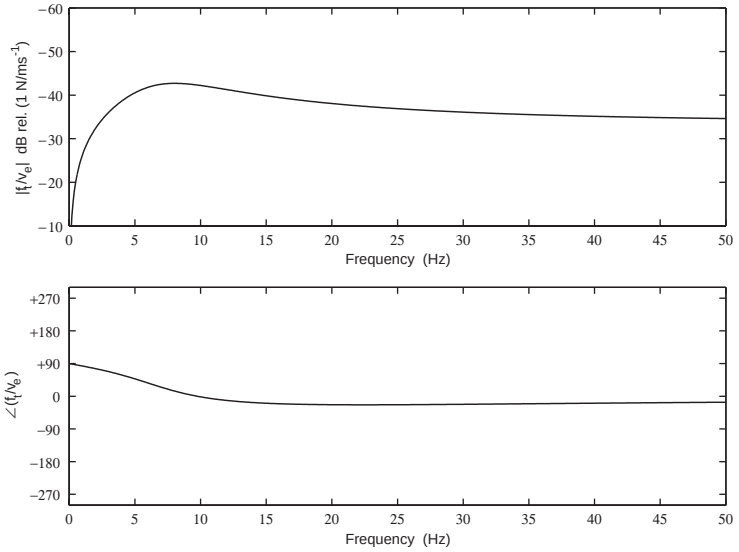

Fig. 19. Impedance of the equipment when the local phase-lag control and the outer velocity feedback control are implemented. $h_{pl} = 100$ and $Z_D = 100$.

5. Experiments with local feedback

Fig. 20 shows the active isolation system used in the experimental work. It consists of an aluminium mass acting as the equipment structure, two mounts placed symmetrically underneath the aluminium mass and one LDS Ling Dynamic Systems V101 electromagnetic shaker to

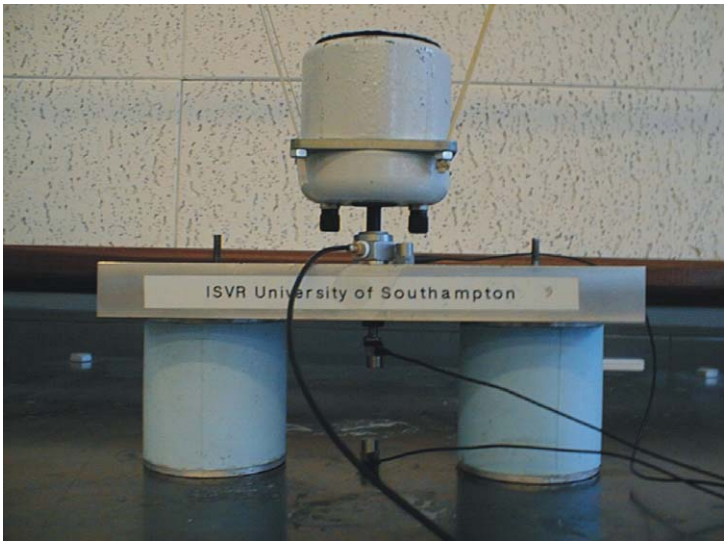

Fig. 20. Experimental set-up.

produce the control force. The case and permanent magnet of the shaker are used as the proof-mass and the shaker is attached to the equipment structure by the coil. The shaker is placed on top of the mass and its weight is held by an external suspension system. This is clearly not a very desirable arrangement in practice, but it does allow a low actuator natural frequency to be achieved with standard laboratory equipment.

The aluminium mass had been previously shown [10] to behave as a rigid body up to 1000 Hz, which is well above the maximum frequency of interest in this experimental study. This system is attached to a flexible plate made of steel. Further details on the passive mount system are given by Gardonio et al. [11] and a complete discussion on the active system is given by Benassi et al. [12]. Accelerometers and force gauges are used as sensors in the positions shown in Fig. 20. When a passive phase-lag compensator is employed as a controller in the local feedback loop, the measured open loop plant response, from command signal to force output as shown in Fig. 21, is in reasonable agreement with Fig. 17. Additional low-frequency phase shifts due to the transducer conditioning electronics cause the experimental Nyquist plot to be rotated anti-clockwise at low frequencies compared with the theoretical predictions, which makes the outer loop only conditionally stable. The spectrum of the measured equipment velocity, normalized by the primary force, is shown in Fig. 22 with no control and with three values of outer velocity feedback gain. The corresponding simulations are shown in Fig. 18.

The experimental measurements are again in reasonable agreement with the theoretical predictions. Below the second cut-off frequency of the phase-lag compensator (22 Hz), the systems behave as if inner integrated force feedback and outer velocity feedback control were implemented, whereas at frequencies higher than 22 Hz, the system behaves as if inner force feedback and outer velocity feedback control were implemented. The maximum attenuation that was obtained in the equipment velocity was about 13 dB, but it should be noted that this was not constrained by stability issues, but was due to gain limitations in the amplifiers that were used. At frequencies below 2 Hz, the data is not meaningful because of low coherence in the measurements.

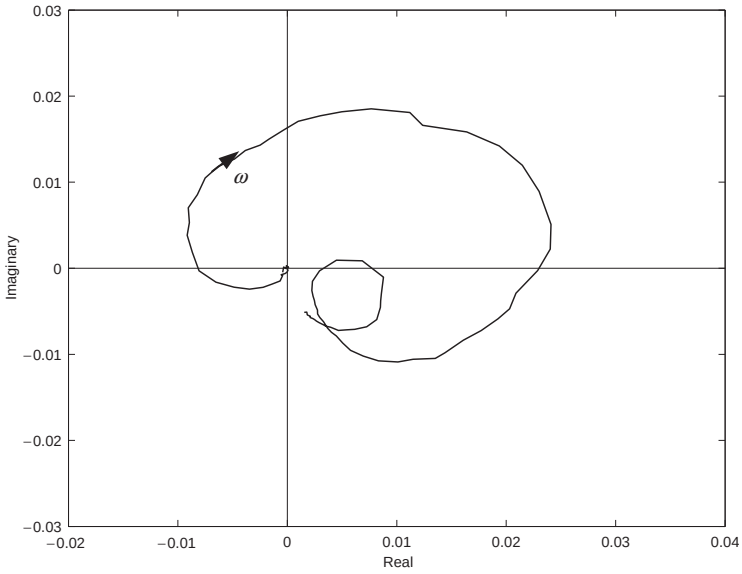

Fig. 21. Nyquist plot of the measured plant response from command signal to integrated accelerometer output when a phase-lag compensator is implemented within the inner feedback loop and $h_{pl} = 100$.

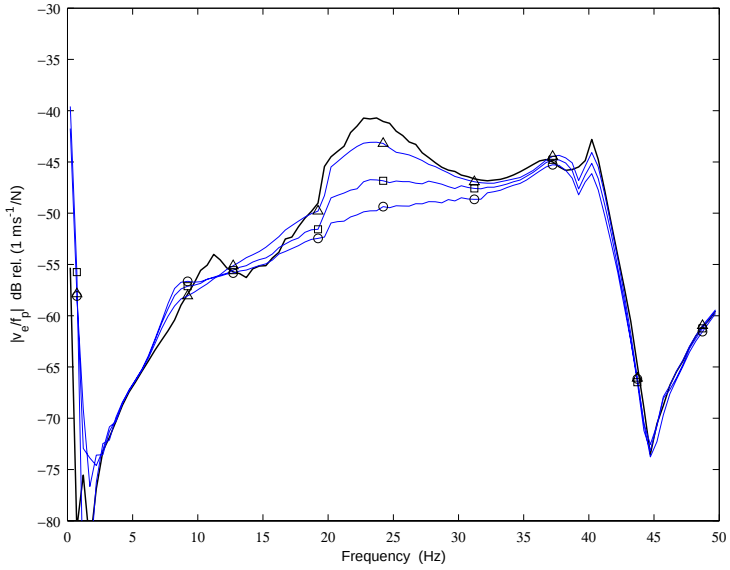

Fig. 22. Measured velocity of the equipment per unit primary excitation. Results are shown for the passive system (control off, solid line) and for three values of the velocity feedback gain in the outer loop (faint lines) when the force feedback gain was set to $h_{pl} = 100$: $Z_D = 20$ (triangle), $Z_D = 50$ (square), and $Z_D = 100$ (circle).

6. Discussions and conclusions

A review of different local feedback loop strategies for active vibration control using an inertial actuator has been presented. Feedback stability margins and performance were considered. The

main finding was that the use of a phase-lag compensator within a local force feedback loop in the inertial actuator is stable and gives an improved actuator response.

A theoretical and experimental investigation of the active vibration isolation of a rigid piece of equipment from a vibrating base structure using the modified inertial actuator was then carried out. The simulation results obtained using a phase-lag compensator within the local feedback loop and a velocity feedback outer loop seem to be very attractive. In order to establish how well this dual-loop control strategy performs compared with an optimal feedback control strategy, some simulations of full state feedback, optimized using LQG control theory, are presented in Appendix A. If the control effort in these simulations is adjusted to be similar to those used by the dual-loop controller, very similar overall attenuations in the equipment velocity are obtained.

The experiments confirmed that large reductions of the equipment velocity, more than 13 dB, can be achieved at its fundamental resonance, together with a very good stability margin. The most important constraints in the use of inertial actuators in active vibration isolation systems are the actuator resonance frequency must be lower than the equipment-dominated resonance frequency and that the actuator resonance must be well damped. An inner force feedback loop can both lower the natural frequency and add considerable damping to the actuator. When the natural frequency of the actuator is low, however, the gravity-induced sag on the actuator's inertial mass will limit the stroke of the actuator.

Appendix A. Equipment isolation of a SDOF system with an inertial actuator using an LQG regulator

In this appendix the performance of a full state feedback controller designed using optimal control theory will be investigated to compare with the performance obtained from the inertial actuator with inner force and outer velocity feedback. The response of the base plate is approximated by that of a single mass spring damper system, as shown in Fig. 23, in order to keep the state-space model simple. The parameters of this model of the base structure were chosen to best approximate the first mode of the base plate. The internal states of the system are given by the

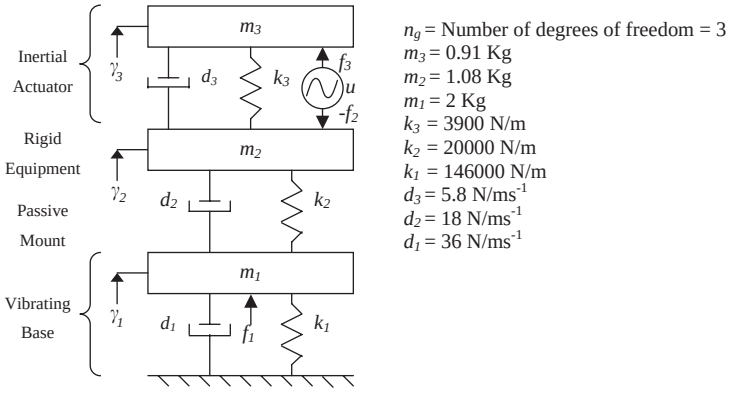

Fig. 23. Schematic of the plant and numerical values used in the simulations of a vibration isolation system with full state feedback control.

displacements of the base mass, equipment mass and actuator mass, γ_1, γ_2, γ_3 and their velocities $\dot{\gamma}_1$, $\dot{\gamma}_2$, $\dot{\gamma}_3$ and the system is driven by the forces f_1, f_2 and f_3. The model of the plant in generalized co-ordinates in Fig. 23 is given by

$$\begin{aligned} m_1\ddot{\gamma}_1 &= f_1 + k_2(\gamma_2 - \gamma_1) - k_1\gamma_1 + d_2(\dot{\gamma}_2 - \dot{\gamma}_1) - d_1\dot{\gamma}_1,\\ m_2\ddot{\gamma}_2 &= f_2 + k_3(\gamma_3 - \gamma_2) - k_2(\gamma_2 - \gamma_1) + d_3(\dot{\gamma}_2 - \dot{\gamma}_1) - d_2(\dot{\gamma}_2 - \dot{\gamma}_1),\\ m_3\ddot{\gamma}_3 &= f_3 - k_3(\gamma_3 - \gamma_2) - d_3(\dot{\gamma}_3 - \dot{\gamma}_2), \end{aligned} \tag{A.1}$$

which can be written as

$$\mathbf{M}\ddot{\boldsymbol{\gamma}}(t) + \mathbf{D}\dot{\boldsymbol{\gamma}}(t) + \mathbf{K}\boldsymbol{\gamma}(t) = \mathbf{f}(t), \tag{A.2}$$

where

$$\mathbf{M} = \operatorname{diag}\{m_1 \quad m_2 \quad m_3\}, \tag{A.3}$$

$$\mathbf{K} = \begin{bmatrix} (k_1+k_2) & -k_2 & 0 \\ -k_2 & (k_2+k_3) & -k_3 \\ 0 & -k_3 & k_3 \end{bmatrix}, \quad \mathbf{D} = \begin{bmatrix} (d_1+d_2) & -d_2 & 0 \\ -d_2 & (d_2+d_3) & -d_3 \\ 0 & -d_3 & d_3 \end{bmatrix} \tag{A.4, A.5}$$

and $\boldsymbol{\gamma}(t) = [\gamma_1(t)\ \gamma_2(t)\ \gamma_3(t)]^{\mathrm{T}}$, $\mathbf{f}(t) = [f_1(t)\ f_2(t)\ f_3(t)]^{\mathrm{T}}$. Multiplying both sides of Eq. (A.2) by $\mathbf{M}^{-1}$, the following equation is obtained:

$$\ddot{\boldsymbol{\gamma}}(t) + \mathbf{M}^{-1}\mathbf{D}\dot{\boldsymbol{\gamma}}(t) + \mathbf{M}^{-1}\mathbf{K}\boldsymbol{\gamma}(t) = \mathbf{M}^{-1}\mathbf{f}(t). \tag{A.6}$$

The state-space model [13], assuming that the system is driven by a disturbance $f_1 = f_p$, controlled by an input u, where $f_2 = u$ and $f_3 = -u$, and the output of the system is given by the equipment velocity $\dot{\gamma}_2 = v_e$, can be written as

$$\begin{aligned} \dot{\mathbf{x}}(t) &= \mathbf{A}\mathbf{x}(t) + \mathbf{B}u(t) + \mathbf{R}f_p(t),\\ \mathbf{y}(t) &= \mathbf{C}\mathbf{x}(t), \end{aligned} \tag{A.7}$$

where

$$\mathbf{x}(t) = \begin{bmatrix} \gamma_1(t) \\ \gamma_2(t) \\ \gamma_3(t) \\ \dot{\gamma}_1(t) \\ \dot{\gamma}_2(t) \\ \dot{\gamma}_3(t) \end{bmatrix}, \quad \mathbf{A} = \begin{bmatrix} \mathbf{0}_{n_g} & \mathbf{I}_{n_g} \\ -\mathbf{M}^{-1}\mathbf{K} & -\mathbf{M}^{-1}\mathbf{D} \end{bmatrix},$$

$$\mathbf{B} = \begin{bmatrix} 0 & 0 & 0 & 0 & \dfrac{-1}{m_2} & \dfrac{1}{m_3} \end{bmatrix}^{\mathrm{T}}, \tag{A.8, A.9, A.10}$$

$$\mathbf{C} = [0 \quad 0 \quad 0 \quad 0 \quad 1 \quad 0], \quad \mathbf{R} = [0 \quad 0 \quad 0 \quad 1/m_1 \quad 0 \quad 0]^{\mathrm{T}}. \tag{A.11, A.12}$$

When the disturbance input is assumed to be white noise and final time of the simulation is assumed to be infinity, the LQG regulator can be obtained by minimizing the

cost function

$$J = \min \int_{t_0}^{\infty} [\mathbf{y}^{\mathrm{T}}(t)\alpha\mathbf{y}(t) + u^{\mathrm{T}}(t)u(t)]\,\mathrm{d}t, \tag{A.13}$$

where changing α provides a family of results depending on the relative importance of reducing the equipment velocity and reducing the control effort. The solution of the LQG problem [13] is given by

$$u(t) = \mathbf{K}\mathbf{x}(t), \tag{A.14}$$

where $\mathbf{K} = -\mathbf{R}^{-1}\mathbf{B}^{\mathrm{T}}\mathbf{S}$ and $\mathbf{S}$ is the unique positive definite solution of the Algebraic Riccati Equation (ARE)

$$\mathbf{S}\mathbf{A} + \mathbf{A}^{\mathrm{T}}\mathbf{S} - \mathbf{S}\mathbf{B}\mathbf{R}^{-1}\mathbf{B}^{\mathrm{T}}\mathbf{S} + \mathbf{C}^{\mathrm{T}}\mathbf{Q}\mathbf{C} = \mathbf{0}. \tag{A.15}$$

If the instabilities are in the controllable part of $(\mathbf{A}, \mathbf{B})$ and the non-observable modes of $(\mathbf{A}, \mathbf{C})$ are stable, then $u(t) = \mathbf{K}\mathbf{x}(t)$ ensures that the system is stable and minimizes the cost function J. In the cases presented below, the non-controllable or non-observable parts of the system are related to the behaviour of the base, which is stable because it is "passive".

It can be noted that $\mathbf{K}$ in Eq. (A.14) is a 1×6 matrix, which assumes that the state vector $\mathbf{x}(t)$ is known at all times. Full state feedback would either require the use of many more than two sensors, or the implementation of a Kalman filter, or state observer, with a very detailed model of the system under control, which makes the stability of the overall feedback system very sensitive to changes in the response of the system [14].

Fig. 24 shows the spectrum of the equipment velocity before any control and with full state feedback calculated to minimize equation (40) with $\alpha = 100$. This can be compared to the

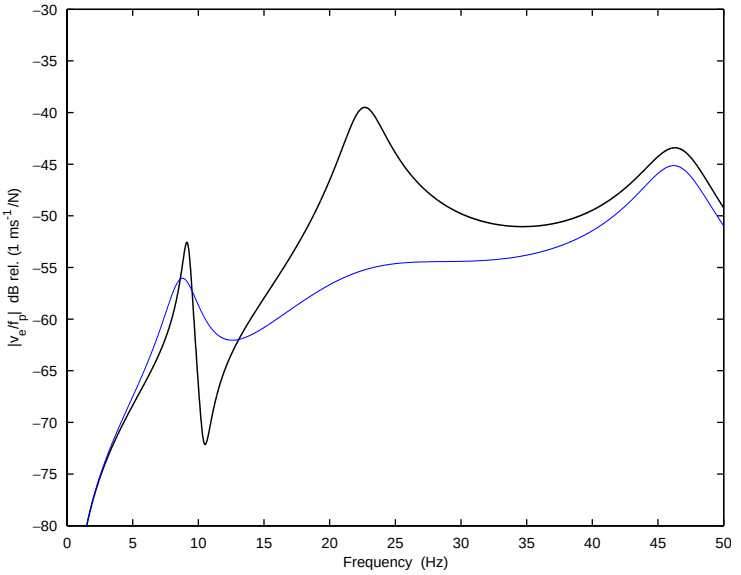

Fig. 24. Bode plot of the equipment velocity per unit primary force when no control is implemented (solid) and when the full state feedback is implemented (faint), optimized using LQG control theory, with a control effort similar to that used to obtain the dual-loop controller shown in Fig. 18 with $Z_D = 50$.

performance in Fig. 18, where a local phase-lag compensator and an outer velocity feedback loop were implemented. This value of α for the optimal controller was chosen so that the control effort was similar to that required for $Z_D = 100$ in Fig. 18. In the optimal control case with $\alpha = 100$, $\mathbf{K} = [-604.3 \quad -2567.1 \quad 1694.8 \quad 13.03 \quad -73.79 \quad -4.62]$. Although the LQ regulator may potentially perform better if α is increased, thanks to the fact that the control force is based on more information, a more complex controller and higher gains are needed to implement such a solution. In conclusion, classical methods based on a local and an outer loop are not only robust, but they also perform well compared to an optimal LQ regulator, requiring a similar control effort.

References

[1] C.E. Crede, Theory of vibration isolation, in: C.M. Harris (Ed.), *Shock and Vibration Handbook*, McGraw-Hill, New York, 1995 (Chapter 30).
[2] E.E. Ungar, Vibration isolation, in: L. Beranek, I.L. Ver (Eds.), *Noise and Vibration Control Engineering*, Wiley, Chichester, 1992 (Chapter 11).
[3] D. Karnopp, Active and semi-active vibration isolation, *American Society of Mechanical Engineers, Journal of Mechanical Designs* 117 (1995) 177–185.
[4] S.J. Elliott, M. Serrand, P. Gardonio, Feedback stability limits for active isolation systems with reactive and inertial actuators, *American Society of Mechanical Engineers, Journal of Vibration and Acoustics* 123 (2001) 250–261.
[5] G.F. Franklin, *Feedback Control of Dynamic Systems*, 3rd Edition, Addison-Wesley, Reading, MA, 1994.
[6] K.A. Ananthaganeshan, M.J. Brennan, S.J. Elliott, High and Low frequency instabilities in feedback control of a single-degree-of-freedom system, *Proceedings of the ACTIVE 2002 Conference*, Southampton, UK, 15–17 July 2002.
[7] L. Benassi, P. Gardonio, S.J. Elliott, Equipment isolation of a SDOF system with an inertial actuator using feedback control strategies, *Proceedings of the ACTIVE2002 Conference*, Southampton, UK, 15–17 July 2002.
[8] L. Benassi, P. Gardonio, S.J. Elliott, Equipment isolation of a SDOF system with an inertial actuator using double feedback control strategies, ISVR Technical Memorandum No. 893, 2002.
[9] D.C. Zimmerman, G.C. Hornar, D.J. Inman, Microprocessor controlled force actuator, *Journal Guidance, Control, and Dynamics* 11 (3) (1988) 230–236.
[10] M. Serrand, Direct Velocity Feedback Control of Equipment Velocity, MPhil Thesis, University of Southampton, 2000.
[11] P. Gardonio, S.J. Elliott, R.J. Pinnington, User manual for the ISVR isolation system with two active mounts for the ASPEN final project experiment, ISVR Technical Memorandum No. 801, 1996.
[12] L. Benassi, S.J. Elliott, P. Gardonio, Equipment isolation of a SDOF system with an inertial actuator using feedback control strategies—Part II: experiment, ISVR Technical Memorandum No. 896, 2002.
[13] K. Zhou, K. Glover, J. Doyle, *Robust and Optimal Control*, McGraw-Hill, New York, 1998.
[14] J.C. Doyle, G. Stein, Robustness with observers, *IEEE Transactions on Automatic Control* AC-24 (1979) 607–611.